The Astrophysical Journal, 1010:218 (6pp), 2026 October 20 https://doi.org/10.3847/1538-4357/aea975
© 2026. The Author(s). Published by the American Astronomical Society.
OPEN ACCESS

A Gamma-Ray-emitting Head–Tail Radio Galaxy Swimming through the Hot Medium of the Merging Cluster A3627

Vaidehi S. Paliya[1], M. Böttcher[2], Swayamtrupta Panda[3,9], Kiran Wani[4], D. J. Saikia[5,6], Mahadev Pandge[7,10], and C. S. Stalin[8]

[1] Inter-University Centre for Astronomy and Astrophysics (IUCAA), SPPU Campus, Pune 411007, India; vaidehi.s.paliya@gmail.com
[2] Centre for Space Research, North-West University, Potchefstroom 2531, South Africa
[3] International Gemini Observatory/NSF NOIRLab, Casilla 603, La Serena, Chile
[4] Indian Institute of Astrophysics, Block II, Koramangala, Bengaluru, Karnataka 560034, India
[5] Fakultat für Physik, Universität Bielefeld, Postfach 100131, D-33501 Bielefeld, Germany
[6] Assam Don Bosco University, Guwahati 781017, Assam, India
[7] Dayanand Science College, Barshi Road, Latur 413512, Maharashtra, India
[8] Indian Institute of Astrophysics, Bengaluru, 560034, India
Received 2026 June 30; revised 2026 September 15; accepted 2026 September 16; published 2026 October 19

Abstract

Head–tail radio sources are jetted active galactic nuclei (AGN) moving through the dense intracluster medium of galaxy clusters. They are extremely rare in the γ-ray sky, likely because they are usually observed at large viewing angles. Therefore, every new γ-ray detection of head–tail radio galaxies allows us to probe the origin of the high-energy emission in this unique class of AGN. Here we report, for the first time, the association of ESO 0137−G007 ($z = 0.016$), a head–tail radio galaxy located at the outskirts of the merging cluster A3627, with the γ-ray source FL16Y J1615.5−6034. The motion of the galaxy through the dense cluster environment and subsequent ram pressure and/or intracluster medium turbulence have led to the formation of a >500 kpc long jet exhibiting a twisted, wiggly radio morphology. Its optical spectrum, obtained with the 4.1 m SOAR telescope, is devoid of emission lines, indicating that the underlying accretion activity is radiatively inefficient. From the measured line-of-sight stellar velocity dispersion, we estimate the mass of the central supermassive black hole to be $(3.36 \pm 1.32) \times 10^9 M_\odot$. We briefly discuss several radiative models to explain the observed broadband spectral energy distribution of ESO 0137−G007. We conclude that deeper multiwavelength observations of this unique γ-ray-emitting head–tail radio galaxy will enable us to better understand the interaction of the jet with the hot cluster environment, thus setting the stage for the research of this class of AGN with the upcoming Square Kilometre Array.

Unified Astronomy Thesaurus concepts: Tailed radio galaxies (1682); Radio galaxies (1343); Gamma-ray astronomy (628); Abell clusters (9)

1. Introduction

High-energy observations of astrophysical sources reveal some of the most intriguing sites where matter and radiation interact. Given the large-scale environments of galaxy clusters, such observations provide tantalizing clues about the dynamics of the cluster gas and its interactions with member galaxies. Some of them exhibit spectacular radio jets which strongly affect the ambient environment (see L. Bîrzan et al. 2020; G. Schellenberger et al. 2023). The radio-emitting plasma is often shaped by the motion of the host galaxy and the ram pressure and/or the large-scale turbulence of the intracluster medium (ICM), leading to the formation of so-called head–tail radio sources (e.g., M. Ryle & M. D. Windram 1968; T. W. Jones & F. N. Owen 1979; B. Sebastian et al. 2017; S. Srivastava & A. K. Singal 2020). A small number of head–tail radio galaxies, e.g., IC 310 ($z = 0.019$), have also been detected at MeV−GeV energies, indicating that their jets are able to accelerate particles to very high energies (M. L. Ahnen et al. 2017; V. S. Paliya et al. 2024, 2025). Since these objects are usually observed at large viewing angles, their rare γ-ray detection makes them a primary target to study the high-energy radiative processes from a different vantage point than the more common beamed jetted active galactic nuclei (AGN) or blazars (see, e.g., Y. Fukazawa et al. 2022; Y.-W. Yu et al. 2024). Recent numerical simulations, involving the evolution of cosmic-ray particle spectra with energy losses and stochastic turbulence acceleration in the jet–wind interaction, also indicate that they are extremely faint γ-ray emitters (T. Ohmura et al. 2023). However, with more than 17 yr of almost uninterrupted monitoring of the γ-ray sky by the Fermi Large Area Telescope (LAT), the potential to identify elusive γ-ray-emitting head–tail radio galaxies remains high.

FL16Y J1615.5−6034 is a γ-ray-emitting source with so far no known associated low-frequency counterpart (S. Abdollahi et al. 2022; J. Ballet et al. 2026). In this paper, we provide observational evidence for the association of FL16Y J1615.5−6034 with the head–tail radio galaxy ESO 0137−G007 ($z = 0.016$) located at the outskirts of the merging cluster A3627 (G. O. Abell et al. 1989). ESO 0137−G007 exhibits an enigmatic >500 kpc long radio jet with a wiggled and twisted morphology, and an arc-shaped radio filament beyond and mostly orthogonal to the collimated inner tail end as revealed by Australian Square Kilometer Array Pathfinder (ASKAP)

[9] Gemini Science Fellow and Visiting astronomer, Cerro Tololo Inter-American Observatory at NSF's NOIRLab, which is managed by the Association of Universities for Research in Astronomy (AURA) under a cooperative agreement with the National Science Foundation.
[10] DST-INSPIRE Faculty.

Original content from this work may be used under the terms of the Creative Commons Attribution 4.0 licence. Any further distribution of this work must maintain attribution to the author(s) and the title of the work, journal citation and DOI.

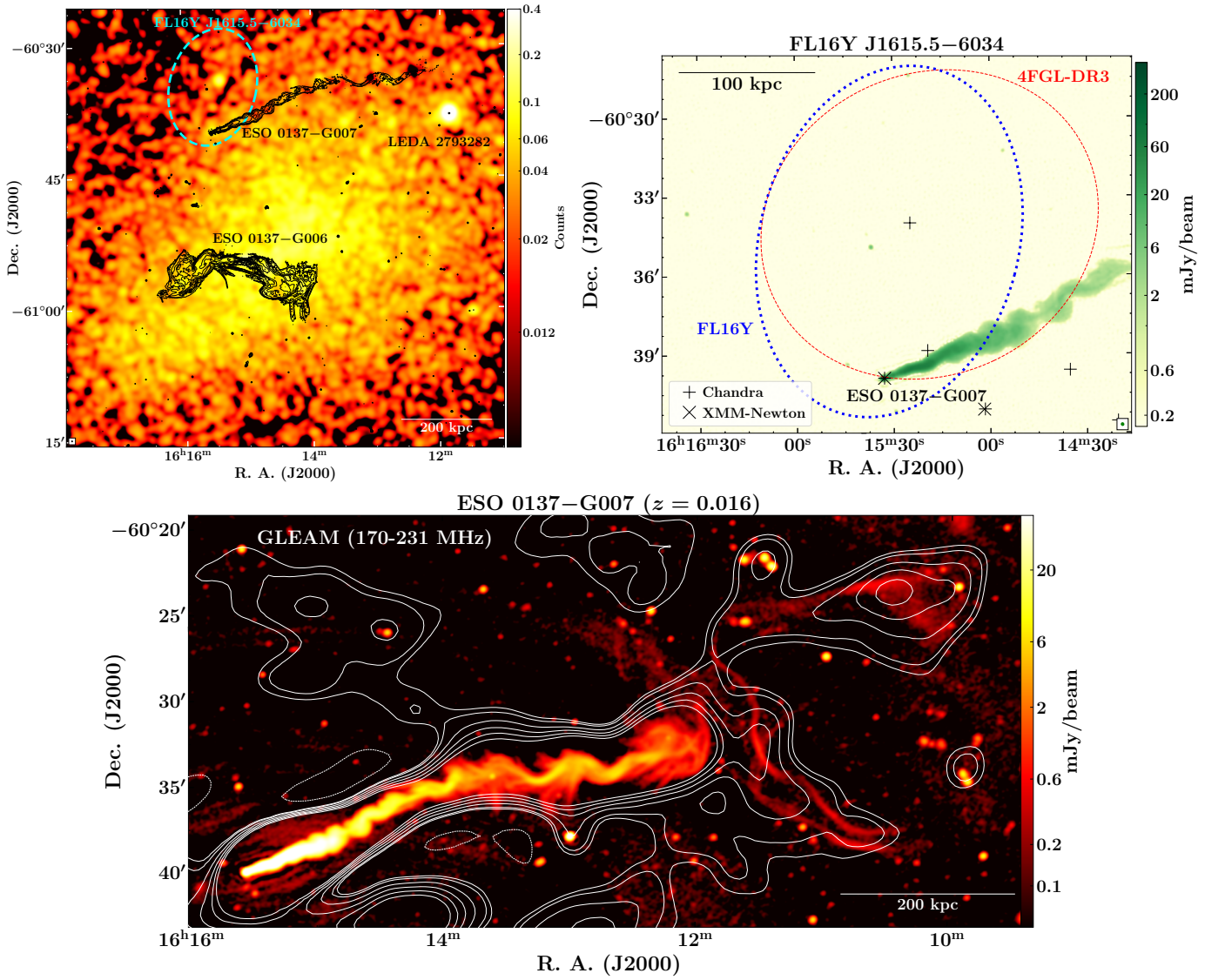


Figure 1. Top left: the 0.2−2.3 keV image of the merging cluster Abell 3627 taken with the eROSITA satellite (A. Merloni et al. 2024). The image is smoothed to highlight the faint diffuse features. Overplotted are the radio contours representing the ASKAP-EMU image. Top right: false-color image of the ASKAP-EMU observation taken at 943 MHz. The plotted ellipses refer to the 95% positional uncertainty in the optimized γ-ray position as provided by the 4FGL-DR3 (red solid ellipse) and FL16Y (blue dotted ellipse) catalogs. The positions of the identified X-ray point sources are also highlighted, as labeled. Bottom: the 170−231 MHz-band contours made using the GaLactic and Extragalactic All-sky MWA (GLEAM) survey (R. B. Wayth et al. 2015) superposed on the ASKAP-EMU image. GLEAM contours are plotted at 0.1, 0.2, 0.3, 0.4, 0.5, and 0.6 Jy beam^{-1}. The image is smoothed to highlight the faint features.

data from the Evolutionary Map of the Universe (EMU; Figure 1; see B. S. Koribalski et al. 2024, for details). The source is traveling eastward close to the plane of the sky, as revealed by the projected radio tail morphology and extent (B. S. Koribalski et al. 2024). From X-ray imaging, it is evident that ESO 0137−G007 plunges through the dense ICM of A3627, and the resulting ram pressure and shear forces sculpt its radio jets (Figure 1, top left panel). Recently, C. Ge et al. (2026) reported the detection of a merger shock (Mach number $\sim$1.3) toward the tail end of the helical jet. All in all, ESO 0137−G007 provides us a unique opportunity to explore the origin of the high-energy emission in what is likely to be a rare γ-ray-emitting head–tail galaxy moving in the dense and hot ICM of a merging cluster.

Throughout, we have adopted the flux density $F_\nu \propto \nu^\alpha$, where α is the radio spectral index. A flat cosmology with $H_0 = 70\,\mathrm{km\,s^{-1}\,Mpc^{-1}}$ and $\Omega_\mathrm{M} = 0.3$ was used.

2. Multiwavelength Association

FL16Y J1615.5−6034 was first reported as a γ-ray source detected at 4.2σ confidence level in the third data release of the fourth catalog of the Fermi-LAT-detected γ-ray sources (4FGL-DR3, named as 4FGL J1615.3−6034; S. Abdollahi et al. 2022). In 4FGL-DR4 and the latest Fermi-LAT 16 yr Source List (FL16Y), it was reported to be detected with 4.46σ and 5.16σ confidence levels, respectively (J. Ballet et al. 2023, 2026). The 0.1−100 GeV energy flux given in the 4FGL-DR3, 4FGL-DR4, and FL16Y catalogs are $(3.45 \pm 0.84) \times 10^{-12}\,\mathrm{erg\,cm^{-2}\,s^{-1}}$, $(3.79 \pm 0.89) \times 10^{-12}\,\mathrm{erg\,cm^{-2}\,s^{-1}}$, and $(3.42 \pm 0.77) \times 10^{-12}\,\mathrm{erg\,cm^{-2}\,s^{-1}}$, respectively. The corresponding power-law photon index values are 2.63 $\pm$ 0.15, 2.67 $\pm$ 0.14, and 2.58 $\pm$ 0.14, respectively. These parameters indicate that FL16Y J1615.5−6034 is a faint but persistent γ-ray emitter with a soft spectrum. In the top right panel of Figure 1, we show the radio image from ASKAP data (800−1088 MHz) centered at the

γ-ray source position and overplot the 95% positional uncertainty ellipses from the 4FGL-DR3 and FL16Y catalogs. While the head–tail galaxy ESO 0137−G007 was barely at the border of the 4FGL-DR3 uncertainty ellipse, it lies well inside the uncertainty ellipse reported in the FL16Y catalog. The FL16Y catalog covered a larger dataset (16 yr) than 4FGL-DR3 (12 yr), and thus has deeper sensitivity, suggesting that ESO 0137−G007 is potentially associated with FL16Y J1615.5−6034. The γ-ray spectral parameters FL16Y J1615.5−6034 are consistent with those found for other γ-ray-detected misaligned jetted AGN (V. S. Paliya et al. 2024), thus providing further supportive evidence for the association.

We explored the possibility of a blazar or other AGN within the 95% uncertainty region of FL16Y J1615.5−6034 as the low-frequency counterpart of the γ-ray object. We found three X-ray point sources considering the objects detected at $>5\sigma$ confidence level in the Chandra Source Catalog and XMM-Newton serendipitous source catalog (N. A. Webb et al. 2020; I. N. Evans et al. 2024). The brightest of them (4XMM J161532.9−603955, $F_{0.2-12\,\mathrm{keV}} = (2.50 \pm 0.47) \times 10^{-13}\,\mathrm{erg\,cm^{-2}\,s^{-1}}$) is positionally consistent with ESO 0137−G007. The other two fainter X-ray sources, 2CXO J161519.3−603852 ($F_{0.5-7\,\mathrm{keV}} = 7.66^{+0.80}_{-0.79} \times 10^{-14}\,\mathrm{erg\,cm^{-2}\,s^{-1}}$) and 2CXO J161524.6−603401 ($F_{0.5-7\,\mathrm{keV}} = 3.17^{+0.52}_{-0.52} \times 10^{-14}\,\mathrm{erg\,cm^{-2}\,s^{-1}}$), are likely to be low-mass stars (H. Yang et al. 2024). Indeed, neither of them is detected in the radio band as revealed by the ASKAP observations (Figure 1, top right panel). A radio point source lies within the γ-ray uncertainty ellipse at R.A. = 243°.90316 and decl. = −60°.58241. However, it is considerably fainter ($F_{1.65\,\mathrm{GHz}} \approx 11$ mJy) than ESO 0137−G007 (core $F_{1.65\,\mathrm{GHz}} \approx 292$ mJy). It is also not detected by the Chandra/XMM-Newton satellites, thus unlikely to be the counterpart of FL16Y J1615.5−6034. Therefore, ESO 0137−G007 is the most promising counterpart of the γ-ray source.

We further quantified the association of ESO 0137−G007 with FL16Y J1615.5−6034 by estimating the multiwavelength likelihood ratio (LR) and computing the Bayesian association probability based on the angular separation from the γ-ray centroid and the surface density of comparable radio and X-ray sources (e.g., W. Sutherland & W. Saunders 1992; M. Salvato et al. 2018). We considered the eROSITA DR1 source catalog (A. Merloni et al. 2024) and Rapid ASKAP Continuum Survey (RACS) source catalog (S. W. Duchesne et al. 2024) to derive per-candidate LR_k as follows:

$$LR_k = \frac{f_k(\Delta x, \Delta y)}{\rho_s(k)}, \tag{1}$$

where $f_k(\Delta x, \Delta y)$ is the spatial Gaussian probability density evaluated at the position of the k^{th} counterpart within the Fermi-LAT error ellipse. The parameter $\rho_s(k)$ is the background number density defined as

$$\rho_s = \frac{n_s}{A},\ s \in \{\mathrm{joint},\ \mathrm{X-rayonly},\ \mathrm{Radioonly}\} \tag{2}$$

for all radio- and/or X-ray-detected objects lying within the background annulus area A. For a given X-ray (F_X) and radio (F_R) flux threshold, we have

$$n_{\mathrm{pairs}} = \#\{(i,j):\ S_{X,i} \geqslant F_X,\ S_{R,j} \geqslant F_R,\ \theta_{ij} \leqslant r_{\mathrm{match}}\} \tag{3}$$

and

$$n_{\mathrm{X/R\text{-}only}} = \#\{i:\ S_{X/R,i} \geqslant F_{X/R}\} - n_{\mathrm{pairs}} \tag{4}$$

where θ_{ij} is the angular separation between the X-ray source i and radio source j, and r_{match} is the crossmatch radius chosen as 3″. The joint calculation used the γ-ray source positional likelihood only once and considered the local density of RACS and eROSITA crossmatched sources satisfying both flux criteria. For ESO 0137−G007, we obtained $f(\Delta x, \Delta y) = 1.28 \times 10^{-6}$ arcsec^{-2}. The background number density was computed within an annulus of inner and outer radii of 0°.1 and 2° centered at the Fermi-LAT source. Taking the radio and X-ray brightness of ESO 0137−G007 as 292 mJy and $2.5 \times 10^{-13}\,\mathrm{erg\,cm^{-2}\,s^{-1}}$, respectively, we derived $\rho_s = 6.15 \times 10^{-9}$ arcsec^{-2}. The normalized separation of the γ-ray source centroid with the RACS and eROSITA positions was found to be 1.91. Inserting these numbers into Equation (1), we estimated the LR to be $\mathcal{LR}_{\mathrm{ESO}} = 208.7$. We also considered X-ray and radio sources, other than ESO 0137−G007, located within the 95% Fermi-LAT uncertainty region. Since the detected X-ray sources have no radio counterparts and vice versa, we conservatively adopted 3σ flux upper limits and derived the LR values of 0.51 (5.5) for only X-ray (radio)-detected objects.

Given N mutually exclusive candidates $k = 1, \ldots, N$ competing for the same Fermi-LAT source, and assuming a single shared prior Q that a true counterpart exists among them at all, the joint multicandidate posterior reliability can be derived as follows (W. Sutherland & W. Saunders 1992):

$$P_k = \frac{LR_k}{\sum_{j=1}^{N} LR_j + \frac{1-Q}{Q}};\ P_{\mathrm{none}} = \frac{\frac{1-Q}{Q}}{\sum_{j=1}^{N} LR_j + \frac{1-Q}{Q}}. \tag{5}$$

Here, P_{none} denotes the probability that none of the considered multiwavelength sources are true counterparts of the γ-ray emitter, thus setting $\sum_{k=1}^{N} P_k + P_{\mathrm{none}} = 1$. Assuming $Q = 0.05$ (see M. Ackermann et al. 2011), we estimated the association probability of ESO 0137−G007 being the low-frequency counterpart of FL16Y J1615.5−6034 to be 89.3%, which is well above the 80% adopted in the Fermi-LAT catalogs (M. Ackermann et al. 2011). For the sources detected only in the radio and X-ray bands, we estimated the association probabilities to be 2.35% and 0.22%, respectively. On the other hand, P_{none} was derived to be 8.13%. Therefore, comparing the association probabilities of all sources, we can conclude ESO 0137−G007 as the most plausible multi-wavelength counterpart of FL16Y J1615.5−6034.

3. Central Engine and Ambient Environment

We procured a new optical spectrum of ESO 0137−G007 using the Goodman High-Transmission Spectrograph (J. C. Clemens et al. 2004) mounted on the 4.1-meter Southern Astrophysical Research Telescope on 2025 May 10 (Program ID: SO2025A-020; co-PI: Panda). We used the M1 Red Camera (400 lines/mm, 0″.45 per pixel) and took three exposures of 600 s each, providing a resolving power of $R \sim 2000$ at 5000 Å and covering a wavelength range of 3900–7000 Å. The detector was operated with a read noise of 3.45 e^- and a gain of 1.54 e^-/ADU in 1 × 1 binning mode. Observations were conducted at an average airmass of 1.17 under stable atmospheric conditions.

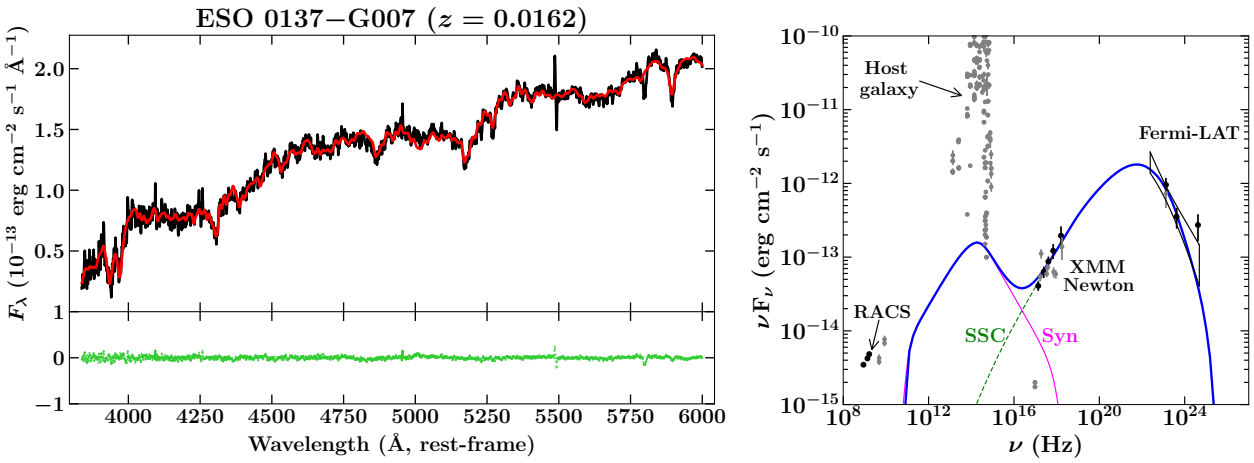


Figure 2. Left: optical spectrum of ESO 0137−G007 taken with the SOAR telescope. The fitted stellar population synthesis model is shown with the red line. Right: the broadband SED of the head–tail radio galaxy reproduced with a stationary single-zone leptonic synchrotron-SSC radiative model. See the text for details.

The data reduction was performed following the standard procedures in the Image Reduction and Analysis Facility (D. Tody 1986). For the flux calibration, we observed the standard star EG 274. In the left panel of Figure 2, we show the observed spectrum, which appears to be consistent with that typically observed from massive elliptical galaxies. No emission lines were detected, implying that the underlying accretion activity is radiatively inefficient. Since the host galaxy absorption features dominate the observed spectrum, we applied the Penalized Pixel Fitting (pPXF) software to determine the line-of-sight stellar velocity dispersion (σ^*; see M. Cappellari & E. Emsellem 2004; M. Cappellari 2023 for details). The fitted model is shown in the left panel of Figure 2, and the σ^* was estimated to be 429.4 ± 14.8 km s^{-1}. Considering the commonly adopted $M - \sigma^*$ relation (e.g., K. Gültekin et al. 2009), we derived the mass of the central supermassive black hole as $(3.36 \pm 1.32) \times 10^9 M_\odot$.

ESO 0137−G007 lies ∼0.3 Mpc (projected) from the center of A3627, a very massive ($M \sim 10^{15} M_\odot$), X-ray–bright cluster at $z = 0.0157$ (R. C. Kraan-Korteweg et al. 1996). Being located close to the Galactic plane, A3627 is highly obscured. Galaxy velocities in the A3627 cluster have a dispersion of order 900 km s^{-1}, indicating it is dynamically evolved but hosts substructure.

4. The Origin of the Broadband Radiation

High-resolution radio observations of head–tail sources suggest that their inner jets are usually not affected by strong relativistic effects, although there are exceptions, as in the case of IC 310 which has also been detected in γ-rays (B. Terni de Gregory et al. 2017; M. Gendron-Marsolais et al. 2020, and references therein). Important characteristics of relativistically beamed emission are (i) a prominent nuclear or core component with a flat radio spectrum, and (ii) significant flux density variability of this component. IC 310 has a flat radio spectrum with $\alpha_{365}^{4850} \sim -0.36$ and its radio emission is dominated by the radio core. From observations at 5 GHz with the Very Large Array, R. J. H. Dunn et al. (2010) reported the peak brightness, which is from the radio core, to be 136 mJy beam^{-1} and its total flux density to be 198 mJy, yielding a core dominance[11] of ∼1.5. IC 310 has exhibited significant X-ray and γ-ray flux variability and has also been found to be variable at radio frequencies (J. Aleksić et al. 2014; M. L. Ahnen et al. 2017; M. Gendron-Marsolais et al. 2020). On VLBI scales it has a core-jet structure similar to blazars (see M. Kadler et al. 2012). On the other hand, the radio spectrum near the core of ESO 0137−G007 is steep (B. S. Koribalski et al. 2024). We also calculated the core dominance using RACS-low data, and found it to be 0.05. This is also likely to be an upper limit as the steep spectrum of the core indicates inclusion of more extended emission in the core flux density. Such a low value of core dominance indicates weak beaming effects, unlike in the case of blazars (M. J. Marchã et al. 2001; Y. Y. Chen et al. 2015; V. S. Paliya et al. 2024). To probe variability of the core in ESO 0137−G007 higher-resolution observations at radio frequencies are required to isolate the core, and higher signal-to-noise data at γ-rays.

Moreover, ESO 0137−G007 does not lie in a region occupied by blazars in the Wide-field Infrared Survey Explorer color–color diagram (also known as WISE blazar strip; F. Massaro et al. 2011). Therefore, available observations do not support the possible beamed nature of the inner radio jet. High-resolution radio observations of this intriguing object will be needed to isolate the core and probe its small-scale structure.

4.1. Broadband Modeling

Given the orientation of the jet approximately perpendicular to our line of sight, radiation models not relying on relativistic Doppler boosting should be considered. The simplest case of such a model is a leptonic single-zone synchrotron-self-Compton model with a stationary emission region. As the infrared—optical—ultraviolet spectrum of the source is dominated by the host galaxy, the synchrotron peak is very poorly constrained. We scale our following estimates by a location at $\nu_{\rm sy} \equiv 10^{14}\,\nu_{\rm sy,14}$ Hz and $\nu F_\nu^{\rm sy} \equiv 10^{-13}\,F_{\rm sy,-13}$ erg cm^{-2} s^{-1}. For a synchrotron self-Compton (SSC) peak at $\nu_{\rm SSC} = 10^{21}\,\nu_{\rm SSC,21}$ Hz, the peak of the radiating electron spectrum is required to be at $\gamma_{\rm e,pk} \sim 3 \times 10^3\,(\nu_{\rm SSC,21}/\nu_{\rm sy,14})^{1/2}$. The peak synchrotron flux provides an estimate of the synchrotron photon energy density in the emission region of $u'_{\rm sy} \sim 4 \times 10^{-7}\,R_{\rm b,pc}^{-2}$ erg cm^{-3}, where the radius of the spherical emission region is parameterized as $R_b \equiv 1\,R_{\rm b,pc}$ pc.

[11] The core dominance is defined as the ratio of the rest-frame core to extended flux densities at 3 GHz (see. e.g., V. S. Paliya et al. 2024).

Table 1
Parameters for the Stationary Leptonic SSC Fit to the SED Shown in Figure 2

Parameter	Symbol	Value
Minimum electron Lorentz factor	$\gamma_{e,min}$	4.7×10^3
Maximum electron Lorentz factor	$\gamma_{e,max}$	3.0×10^5
Electron spectral index	q_e	3.0
Escape timescale parameter	η_{esc}	100
Magnetic field	B	2 G
Bulk Lorentz factor	Γ	1.1
Viewing angle	θ_{obs}	80°
Blob radius	R	1.0×10^{15} cm
Derived Quantities		
Electron luminosity	L_e	4.3×10^{42} erg s^{-1}
Magnetic field luminosity	L_B	1.8×10^{40} erg s^{-1}
Ratio of magnetic field to electron energy densities	u'_B/u'_e	4.2×10^{-3}

For an SSC peak flux of $\nu F_\nu^{SSC} \sim 2 \times 10^{-12}$ erg cm^{-2} s^{-1}, the ratio of SSC to synchrotron peak fluxes constrains the magnetic field through the identity $u'_{sy}/u'_{SSC} = \nu F_\nu^{sy}/\nu F_\nu^{SSC}$ to be $B \sim 7 \times 10^{-4}\, R_{b,pc}^{-1}$ G. Finally, to produce a synchrotron peak at $\nu_{sy} \sim 4 \times 10^6\, B_G\, \gamma_{e,pk}^2$ Hz $\sim 3 \times 10^{10}\, (\nu_{SSC,21}/\nu_{sy,14})\, R_{b,pc}^{-1}$Hz $\sim 10^{14}$ Hz, we require $R_{b,pc} \sim 3 \times 10^{-4}$, i.e., a very small emission region of radius $R_b \sim 10^{15}$ cm, which then implies a magnetic field strength of $B \sim 2$ G.

In order to test the viability of a stationary SSC model with parameters as estimated above, we employ the leptonic blazar emission model of M. Böttcher et al. (2013), with bulk Lorentz factor $\Gamma = 1.1$ and viewing angle $\theta_{obs} = 80°$, i.e., negligible Doppler boosting. We caution that the choice of a viewing angle of 80° is a model assumption and not an observationally established value. Moreover, given the poor quality data, especially in the infrared–ultraviolet region, the model used here should be considered as an illustrative SSC realization rather than a statistically constrained fit. The code assumes continuous injection of a nonthermal, relativistic electron distribution, described by a power law with low- and high-energy cutoffs at $\gamma_{min/max}$, respectively. A tangled magnetic field is assumed, and for the SSC case, external target radiation fields for Compton scattering are neglected. The code evaluates an equilibrium between the above-mentioned particle injection, radiative (synchrotron + SSC) cooling, and escape on a timescale $t_{esc} = \eta_{esc} R_b/c$. Specific parameters employed are listed in Table 1, and the resulting SSC model fit is shown in in the right panel of Figure 2.

The parameters listed in Table 1 appear reasonable and consistent with electrons energized by shock acceleration in a small region in which the jet interacts with its external environment. The small emission-region size required suggests that it is located very close to the central engine, and the very low magnetization appears to favor the formation of strong shocks, favoring shock acceleration as the dominant acceleration mechanism.

We also explored the possibility of an external-Compton (EC) emission. As there is no indication in the spectral energy distribution (SED) for a strong accretion-disk (or broad-line region (BLR)) radiation field, the dominant external radiation field for which there is observational evidence is that of the host galaxy, which, however, is likely to be distributed over (at least) kpc scales. Scaling estimates in terms of $R_{ext} \equiv 1\, R_{ext,kpc}$ kpc, this implies an external radiation field of order $u_{ext} \sim 10^{-11}\, R_{ext,kpc}^{-2}$ erg cm^{-3}. The synchrotron-to-γ-ray-flux ratio then implies a magnetic field of $B \sim 5 \times 10^{-6}\, R_{ext,kpc}^{-1}$ G. The ratio of EC to synchrotron peak frequencies then implies the same estimate for γ_e as for the SSC scenario above, which then, however, leads to a synchrotron peak at $\nu_{sy} \sim 2 \times 10^8\, R_{ext,kpc}^{-1}$ Hz, clearly incompatible with the observed radio spectrum. We therefore conclude that an unbeamed EC model without additional (not directly constrained) external radiation fields is implausible.

5. Summary

ESO 0137−G007, a Fanaroff–Riley Type I (B. L. Fanaroff & J. M. Riley 1974) radio galaxy with a head–tail structure in a merging cluster, has added to the rich variety of misaligned AGN which have been detected in γ-rays in recent years (e.g., G. Bruni et al. 2022; V. S. Paliya et al. 2024, 2025; G. Bruni et al. 2026). These include compact symmetric objects, other Fanaraoff-Riley Type Is (FRIs) including wide-angle tailed sources and FR0s, and giant radio galaxies. Finding a head–tail radio galaxy as a counterpart of an unidentified γ-ray source indicates the importance of sensitive wide-field radio surveys. About a third of all known γ-ray sources are still unidentified (J. Ballet et al. 2026). Therefore, recent discoveries, including this work, have demonstrated that misaligned AGN might be more numerous in the γ-ray band than previously thought (G. Bruni et al. 2022, 2026). Clearly, SKA will reveal many more such objects, thus improving the counterpart classification of unknown γ-ray sources. This will also trigger high-resolution multiwavelength follow-up observations to explore the jet orientation, the origin of the high-energy emission, and the dynamical nature of the systems.

Although the γ-ray emission from ESO 0137−G007 can be understood in terms of the leptonic SSC model with electrons accelerated over a small region, the rich variety of misaligned γ-ray AGN suggests the possible coexistence of external inverse-Compton processes on different scales with photon fields from the host galaxy, extragalactic background light or the cosmic microwave background (e.g., M. Persic & Y. Rephaeli 2020 and references therein), and possible hadronic contributions in dense fields. Our model-dependent results hint that a stationary SSC model can possibly explain the broadband SED. However, the γ-ray emission from a few nearby misaligned AGN, such as Cen A and NGC 6251, has also been explained due to the inverse-Compton scattering of the cosmic microwave background radiation. With deeper multiwavelength observations, as done for Cen A and NGC 6251, it will be possible to better constrain the γ-ray production mechanism in ESO 0137−G007. High-resolution very-long-baseline interferometric observations will also permit us to check for superluminal motion and estimate the viewing angle accurately.

A detailed understanding of the physical processes would require deep imaging to determine the structure and extent of the radio emission and SED modeling. The tail in ESO 0137−G007 has been seen to extend >500 kpc. While SKA-low will provide unprecedented surface-brightness sensitivity to diffuse emission even from possible earlier cycles of jet activity, SKA-mid, along with VLBI networks, will help determine the small-scale structure and help understand the

origin of their γ-ray emission. The SKA will be complemented by the NewAthena X-ray observatory, the Cherenkov Telescope Array Observatory, and the neutrino telescopes IceCube-Gen2 and KM3NeT to provide a more complete understanding of γ-ray-emitting misaligned AGN.

Acknowledgments

We thank the journal referee for constructive criticism. M.B. P. gratefully acknowledges the support from the Science and Engineering Research Board (SERB), New Delhi, under the "SERB CRG" funding with sanction No. CRG/2023/003463. This paper includes archived data obtained through the CSIRO ASKAP Science Data Archive (CASDA) (https://data.csiro.au). This paper is based on observations obtained at the Southern Astrophysical Research (SOAR) telescope, which is a joint project of the Ministério da Ciência, Tecnologia e Inovações (MCTI/LNA) do Brasil, the US National Science Foundation's NOIRLab, the University of North Carolina at Chapel Hill (UNC), and Michigan State University (MSU). We are grateful to Drs. Denimara Dias dos Santos (LNA, Brazil) and Alberto Rodríguez Ardila (ON, Brazil) for granting access to their observing time on SOAR to observe this source. S.P. is supported by the international Gemini Observatory, a program of NSF NOIRLab, which is managed by the Association of Universities for Research in Astronomy (AURA) under a cooperative agreement with the U.S. National Science Foundation, on behalf of the Gemini partnership of Argentina, Brazil, Canada, Chile, the Republic of Korea, and the United States of America.

ORCID iDs

Vaidehi S. Paliya https://orcid.org/0000-0001-7774-5308
M. Böttcher https://orcid.org/0000-0002-8434-5692
Swayamtrupta Panda https://orcid.org/0000-0002-5854-7426
Kiran Wani https://orcid.org/0000-0003-0841-7823
D. J. Saikia https://orcid.org/0000-0002-4464-8023
Mahadev Pandge https://orcid.org/0000-0002-9699-6257
C. S. Stalin https://orcid.org/0000-0002-4998-1861

References

Abdollahi, S., Acero, F., Baldini, L., et al. 2022, ApJS, 260, 53
Abell, G. O., Corwin, H. G., Jr., & Olowin, R. P. 1989, ApJS, 70, 1
Ackermann, M., Ajello, M., Allafort, A., et al. 2011, ApJ, 743, 171
Ahnen, M. L., Ansoldi, S., Antonelli, L. A., et al. 2017, A&A, 603, A25
Aleksić, J., Antonelli, L. A., Antoranz, P., et al. 2014, A&A, 563, A91
Ballet, J., Bruel, P., Burnett, T. H., & Lott, B. 2026, arXiv:2602.22148
Ballet, J., Bruel, P., Burnett, T. H., Lott, B. & The Fermi-LAT collaboration 2023, arXiv:2307.12546
Bîrzan, L., Rafferty, D. A., Brüggen, M., et al. 2020, MNRAS, 496, 2613
Böttcher, M., Reimer, A., Sweeney, K., & Prakash, A. 2013, ApJ, 768, 54
Bruni, G., Bassani, L., Persic, M., et al. 2022, MNRAS, 513, 886
Bruni, G., Paliya, V. S., Saikia, D. J., et al. 2026, in Advancing Astrophysics with the SKA II, ed. A. Bonaldi et al. (Square Kilometer Array Observatory), 79
Cappellari, M. 2023, MNRAS, 526, 3273
Cappellari, M., & Emsellem, E. 2004, PASP, 116, 138
Chen, Y. Y., Zhang, X., Zhang, H. J., & Yu, X. L. 2015, MNRAS, 451, 4193
Clemens, J. C., Crain, J. A., & Anderson, R. 2004, SPIE, 5492, 331
Duchesne, S. W., Grundy, J. A., Heald, G. H., et al. 2024, PASA, 41, e003
Dunn, R. J. H., Allen, S. W., Taylor, G. B., et al. 2010, MNRAS, 404, 180
Evans, I. N., Evans, J. D., Martínez-Galarza, J. R., et al. 2024, ApJS, 274, 22
Fanaroff, B. L., & Riley, J. M. 1974, MNRAS, 167, 31P
Fukazawa, Y., Matake, H., Kayanoki, T., Inoue, Y., & Finke, J. 2022, ApJ, 931, 138
Ge, C., Sun, M., Ramatsoku, M., Nolting, C., & Koribalski, B. S. 2026, ApJ, 1000, 67
Gendron-Marsolais, M., Hlavacek-Larrondo, J., van Weeren, R. J., et al. 2020, MNRAS, 499, 5791
Gültekin, K., Richstone, D. O., Gebhardt, K., et al. 2009, ApJ, 698, 198
Jones, T. W., & Owen, F. N. 1979, ApJ, 234, 818
Kadler, M., Eisenacher, D., Ros, E., et al. 2012, A&A, 538, L1
Koribalski, B. S., Duchesne, S. W., Lenc, E., et al. 2024, MNRAS, 533, 608
Kraan-Korteweg, R. C., Woudt, P. A., Cayatte, V., et al. 1996, Natur, 379, 519
Marchã, M. J., Caccianiga, A., Browne, I. W. A., & Jackson, N. 2001, MNRAS, 326, 1455
Massaro, F., D'Abrusco, R., Ajello, M., Grindlay, J. E., & Smith, H. A. 2011, ApJL, 740, L48
Merloni, A., Lamer, G., Liu, T., et al. 2024, A&A, 682, A34
Ohmura, T., Asano, K., Nishiwaki, K., Machida, M., & Sakemi, H. 2023, ApJ, 951, 76
Paliya, V. S., Saikia, D. J., Bruni, G., Domínguez, A., & Stalin, C. S. 2025, ApJ, 989, 36
Paliya, V. S., Saikia, D. J., Domínguez, A., & Stalin, C. S. 2024, ApJ, 976, 120
Persic, M., & Rephaeli, Y. 2020, MNRAS, 491, 5740
Ryle, M., & Windram, M. D. 1968, MNRAS, 138, 1
Salvato, M., Buchner, J., Budavári, T., et al. 2018, MNRAS, 473, 4937
Schellenberger, G., O'Sullivan, E., Giacintucci, S., et al. 2023, ApJ, 948, 101
Sebastian, B., Lal, D. V., & Pramesh Rao, A. 2017, AJ, 154, 169
Srivastava, S., & Singal, A. K. 2020, MNRAS, 493, 3811
Sutherland, W., & Saunders, W. 1992, MNRAS, 259, 413
Terni de Gregory, B., Feretti, L., Giovannini, G., et al. 2017, A&A, 608, A58
Tody, D. 1986, SPIE, 627, 733
Wayth, R. B., Lenc, E., Bell, M. E., et al. 2015, PASA, 32, e025
Webb, N. A., Coriat, M., Traulsen, I., et al. 2020, A&A, 641, A136
Yang, H., Hare, J., & Kargaltsev, O. 2024, ApJ, 971, 180
Yu, Y.-W., Zhang, H.-M., Gan, Y.-Y., et al. 2024, ApJ, 965, 163